analytical chemistry

Article

pubs.acs.org/ac

Self-Referencing Optofluidic Ring Resonator Sensor for Highly Sensitive Biomolecular Detection

Ming Li,[†,§] Xiang Wu,[†,§] Liying Liu,[†] Xudong Fan,*[,†,‡] and Lei Xu*[,†]

[†]Key Laboratory for Micro and Nano Photonic Structures (Ministry of Education), Department of Optical Science and Engineering, Fudan University, Shanghai 200433, People's Republic of China

[‡]Department of Biomedical Engineering, University of Michigan, Ann Arbor, Michigan 48109, United States

Supporting Information

ABSTRACT: The noise-suppression techniques of label-free optical ring resonator sensors are crucial to improve their practical sensing capabilities for biochemical analysis and detection in extremely small detection concentration. We have developed a self-referencing optofluidic ring resonator (SR-OFRR) to vastly improve its sensing capability as a label-free optical biosensor. By monitoring the mode-splitting separation generated on a coupled ring resonator system, the common-mode noise is suppressed by 2 orders of magnitude without any external noise-suppression techniques. In this work, we first carried out theoretical analysis to elucidate the sensing principle and then applied the SR-OFRR biosensor to experimentally detect bovine serum albumin with a concentration detection limit on the order of 1 pg/mL (~15 fM).

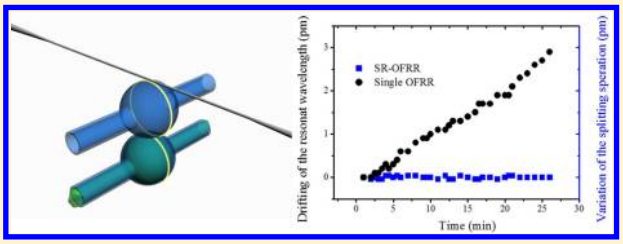

Optical ring resonators have been intensely investigated for highly sensitive label-free chemical and biological sensing in the past decade.[1−6] In an optical ring resonator, the whispering gallery mode (WGM) forms due to total internal reflection of light along its curved surface. The WGM spectral position is sensitive to the refractive index change arising from the binding of chemical and/or biological molecules to the resonator surface, and therefore, the WGM spectral shift is often used as the sensing signal. The ring resonator has high *Q*-factors, ranging from 10^4 to 10^7 orders of magnitude higher than those of any other label-free biosensors.[7] Such a high *Q*-factor translates to an extremely narrow spectral line width, which leads to a low noise in determining the WGM spectral position.

However, the WGM spectral position is susceptible to many other forms of noise, in particular common-mode noises, such as temperature fluctuation of the ring resonator and frequency jittering of the interrogation laser. Those forms of noise cause the WGM spectral position to drift and unfortunately cannot be suppressed by resorting to a higher *Q*-factor (or a narrower line width). Recent theoretical analysis shows that an excessive *Q*-factor does not necessarily result in a lower noise in the sensing signal (i.e., WGM spectral shift).[7] In practice, when a *Q*-factor is higher than 10^5, the common-mode noises become dominant and form the bottleneck that limits the ring resonator sensing performance.[5]

To further improve the detection limit, temperature or frequency stabilization methods (generally by a thermally controlled copper chamber[8] or a calibrated probe laser jitter[9]) are employed. However, temperature/frequency stabilization is complicated and slow and often involves bulky instruments. Optical self-referencing techniques provide an excellent means for common-mode noise suppression and have the advantages of being simple, compact, rapid, and efficient. Self-referencing has been employed in the development of various types of label-free biosensors such as dual-wavelength surface plasmon resonance biosensors and Mach−Zehnder interferometer biosensors.[10−12] Recently, the self-referencing detection method has been applied to a single toroidal ring resonator, where the mode splitting caused by the interaction between the clockwise and counterclockwise WGMs was used as the sensing signal.[13−15] As the mode splitting is immune to those common-mode noises, single nanoparticles tens of nanometers in diameter have successfully been detected. Despite its outstanding sensing performance in detecting single particles, the splitting mode method on a single-ring resonator has an intrinsic limitation, as the sensing signal (i.e., the change in the mode splitting) is quasi-random and is highly dependent upon the history of particle attachment prior to the particle being measured. Apparently, such behavior renders this type of sensor nearly useless when multiple biomolecules are expected to attach to the resonator surface simultaneously in typical biosensing measurement. Furthermore, the sensing signal initially increases and then progressively decreases with the increased amount of biomolecules attached to the sensor surface and eventually reaches zero (i.e., no additional mode splitting compared to before biomolecular attachment) when a full layer of biomolecules are attached to the ring resonator.

Received: July 16, 2013
Accepted: August 30, 2013
Published: August 30, 2013

   dx.doi.org/10.1021/ac402174x | *Anal. Chem.* 2013, 85, 9328−9332

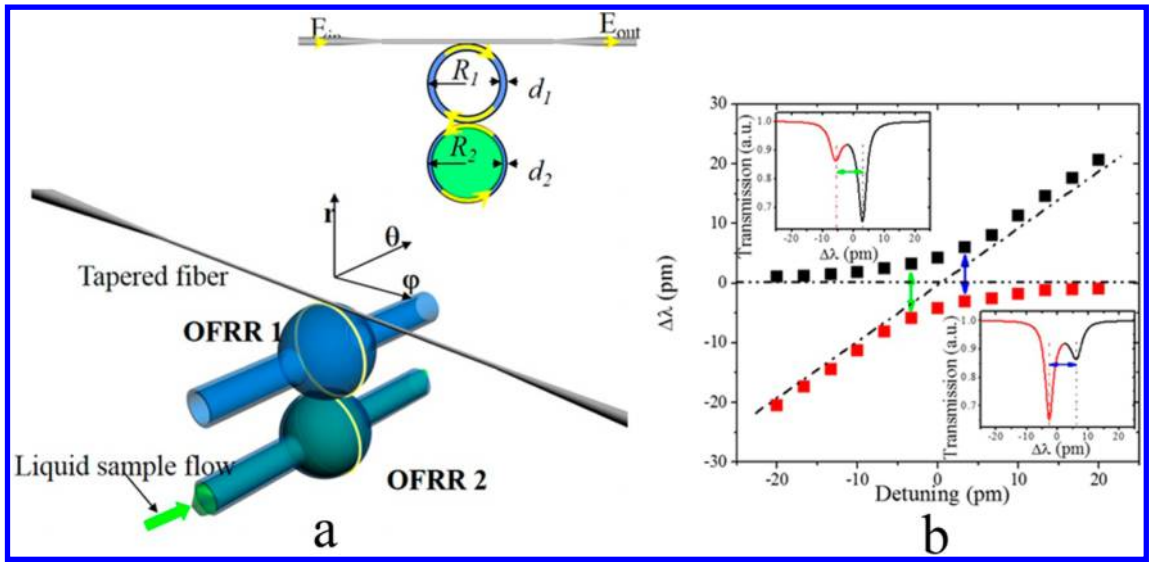

Figure 1. Principle of an SR-OFRR biosensor. (a) Schematic of an SR-OFRR biosensor. OFRR 1 acts as the reference resonator, while OFRR 2 serves as the sensing resonator. (b) Theoretical mode splitting in an SR-OFRR biosensor with resonance detuning. The red and black squares represent the left and right branches of the modes, respectively. The vertical axis denotes the relative wavelength of the branches with respect to the zero point, which is set at the resonance wavelength of OFRR 1.

Both shortcomings make quantification of analytes almost impossible. Here we developed a self-referencing optofluidic ring resonator (SR-OFRR) biosensor that can substantially reduce the common-mode noise while still having a high *Q*-factor and respond deterministically to the attachment of biomolecules to the resonator surface. Both merits enable accurate quantification of analytes with an unprecedented detection limit.

MATERIALS AND METHODS

Principle of the SR-OFRR Sensors. The SR-OFRR structure is illustrated in Figure 1a. It consists of two capillary-based ring resonators in contact at their equators. The WGMs of each ring resonator interact with one another, and mode splitting occurs when the two WGMs are on or near resonance, as seen in the transmission spectrum at the distal end of the fiber. Figure 1b shows the theoretical mode splitting in an SR-OFRR biosensor when the resonance of OFRR 1 is fixed while the resonance of OFRR 2 is detuned from −20 to +20 pm with respect to that of OFRR 1. The mode splitting changes with various detunings.[16] By monitoring the magnitude of the mode splitting in an SR-OFRR, an ultralow quantity of biomolecules attached to one of the OFRRs, which leads to the resonance detuning, can be detected precisely.

Fabrication of the SR-OFRR Sensors. The OFRRs were fabricated by the localized electrical discharge heat of pressurized silica capillaries (Figure 2a).[17] First, we pre-etched a silica capillary (Polymicro TSP100160) with an outer diameter (o.d.) of 140 μm and an inner diameter (i.d.) of 100 μm from the inside by hydrofluoric acid (HF). Second, one end of the capillary was sealed with a fusion splicer (Ericsson FSU 975), while the other side was connected to a syringe pump, which was used to control the air pressure inside the capillary. After the capillary was heated by the fusion splicer, OFRRs of various diameters and wall thicknesses could be obtained under a proper air pressure (Supporting Information, section I). Then two OFRRs fabricated by this method were placed in contact at the equators by precision fiber-optic alignment stages. One OFRR acted as the reference resonator

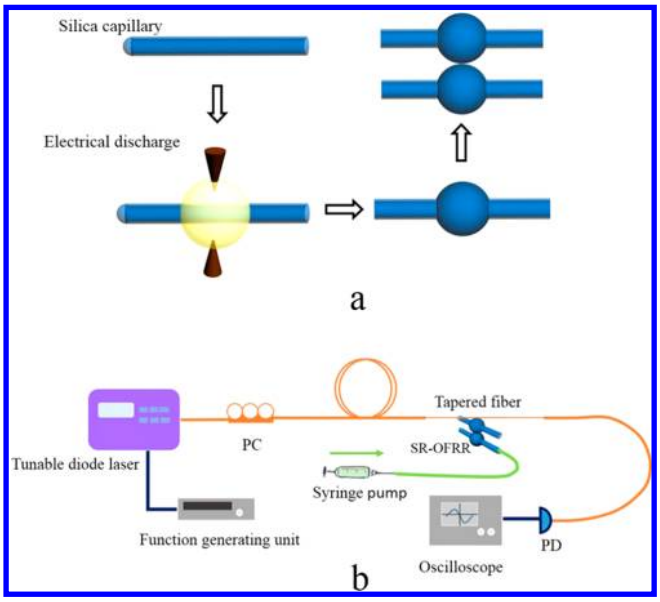

Figure 2. (a) Fabrication of an SR-OFRR biosensor. The individual OFRRs were first fabricated by the fuse-and-blow technique, and then the two OFRRs were placed in contact with each other at their equators. (b) Experimental setup. Light from a tunable laser was coupled into the SR-OFRR via a 2 μm tapered fiber, and the transmission signal was sent to a photon detector. PC = polarization controller, and PD = photodetector.

(OFRR 1), which was kept empty, while the other served as the sensing resonator and microfluidic channel (OFRR 2), which was connected with Teflon tubes. Finally, HF solution (0.1%) was pumped (Harvard, Pump 11 Elite syringe pump series) through OFRR 2 again, which reduced the wall thickness to 2.5 μm (Supporting Information, section II) at an etching rate of 1.2 nm/min.

Experimental Setup. The experimental setup is illustrated as shown in Figure 2b. In our experiments, light from a tunable laser (λ = 840 nm, New Focus TBL-6716) was coupled into the SR-OFRR via a 2 μm tapered fiber and the transmission signal

dx.doi.org/10.1021/ac402174x | *Anal. Chem.* 2013, 85, 9328−9332

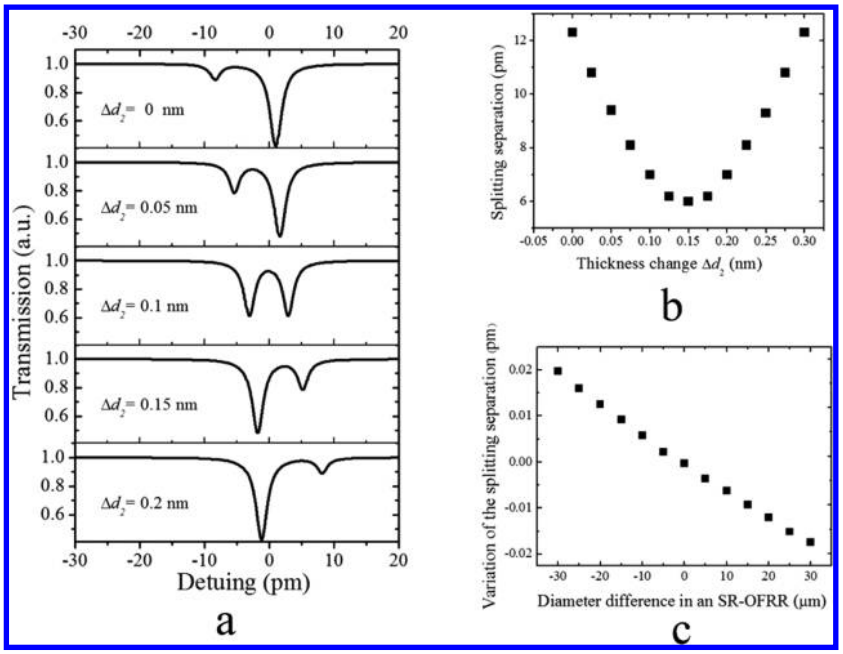

Figure 3. (a) Transmission spectra for an increase of 0.05 nm in the OFRR 2 diameter. The resonance wavelength of OFRR 2, 840 nm, is set to be the zero point in the *x*-axis. (b) Mode splitting for various changes in the OFRR wall thickness. (c) Variation of the mode splitting as a function of the diameter difference between OFRR 1 and OFRR 2 when the temperature changes by 1 °C. The diameter of OFRR 1 is fixed at 140 μm, and the diameter of OFRR 2 is varied from 110 to 170 μm.

was sent to a photon detector (PD). The function generator unit repeatedly scanned the laser wavelength around the split modes across a wavelength range of 120 pm. The transmission signal was monitored by an oscilloscope connected to the PD. Note that no external noise-suppression techniques were employed in the system.

Biomolecular Detection Method. For the capture of bovine serum albumin (BSA) molecules, the inner surface of OFRR 2 was silanized by flowing 2% (aminopropyl)-trimethylsilane (APTMS) in water though OFRR 2 by 45 min and then thorough rinsing with deionized (DI) water. Finally, the OFRR 2 was filled with DI water and ready for detection. The BSA solution with various concentrations was then pumped through OFRR 2. Note that all measurements were performed at room temperature and the solution was withdrawn into the OFRR at a flow rate of 10 μL/min with a peristaltic pump during the measurements.

RESULTS AND DISCUSSION

Theoretical Analysis. We first conducted theoretical analysis in Figure 3a of the SR-OFRR mode splitting when biomolecules are attached to the OFRR inner surface, which can be simulated by varying the wall thickness, d_2, of OFRR 2. The power transmission can be expressed as[18,19] (Supporting Information, section III)

$$T = \left|\frac{E_{out}}{E_{in}}\right|^2 = \left|\frac{r_1 - e^{-\alpha_1 L_1/2} e^{i\delta_1}\Theta(\delta_2, \alpha_2)}{1 - r_1 e^{-\alpha_1 L_1/2} e^{i\delta_2}\Theta(\delta_2, \alpha_2)}\right|^2 \quad (1)$$

where

$$\Theta(\delta_2, \alpha_2) = \frac{r_2 - e^{-\alpha_2 L_2/2} e^{i\delta_2}}{1 - r_2 e^{-\alpha_2 L_2/2} e^{i\delta_2}} \quad (2)$$

is the complex electric field transmission for the reference resonator (OFRR 1) coupled with the tapered fiber. $\delta_j = (2\pi n_j^{\mathrm{eff}(m,l)} L_j)/\lambda$ is the round trip phase shift. L_j is the circumference of the OFRR at the equator, and λ is the wavelength. j = 1 or 2 denotes OFRR 1 or 2. $n_j^{\mathrm{eff}(m,l)}$ is the effective refractive index with azimuthal index m and radial index l of each resonator. α_j is the absorption coefficient, r_1 and r_2 are the reflection coefficients between the tapered fiber and OFRR 1 and between OFRR 1 and OFRR 2, respectively. Since the mode splitting varies with the coupling interference states between the two OFRRs, detection of small effective RI changes in OFRR 2 can be accomplished by monitoring the mode splitting change. In the theoretical analysis for biomolecular binding, assuming that the two OFRRs have the same radius of 140 μm, the thickness of OFRR 1, d_1, is fixed at 2.662 μm and the initial d_2 is set as 2.500 μm. OFRR 1 is kept empty, and OFRR 2 is filled with water of n_{core} = 1.33. The other parameters are set as r_1 = 0.999900, α_1 = 0.000005, r_2 = 0.999999, and α_2 = 0.000050. The resonant wavelength around 840 nm is considered in this case.

When d_2 changes, the resonance wavelength of OFRR 2 moves relative to that of OFRR 1; thus, resonance detuning is generated between the two OFRRs. At the beginning, as shown in Figure 3b, the mode splitting decreases with increased thickness d_2 and then reaches the minimum value of 6.0 pm at zero detuning, where the two OFRRs are on resonance. After the minimum point, the mode splitting increases with a surface thickness sensitivity of 40 pm/nm. Assuming a spectral resolution of 0.025 pm (see later text), a detection limit of a 0.34 pm thick biomolecular layer (assuming the refractive index of a biomolecule layer is 1.55) can be achieved. For protein molecules of about 3 nm, the above detection limit translates to a surface mass density of 0.26 pg/mm^2.

We further investigated theoretically the thermal stability of the SR-OFRR to the environmental temperature fluctuation. Figure 3c shows the variation of the mode splitting as a function of the diameter difference between OFRR 1 and OFRR 2 when the temperature changes by 1 °C. If the two

dx.doi.org/10.1021/ac402174x | Anal. Chem. 2013, 85, 9328−9332

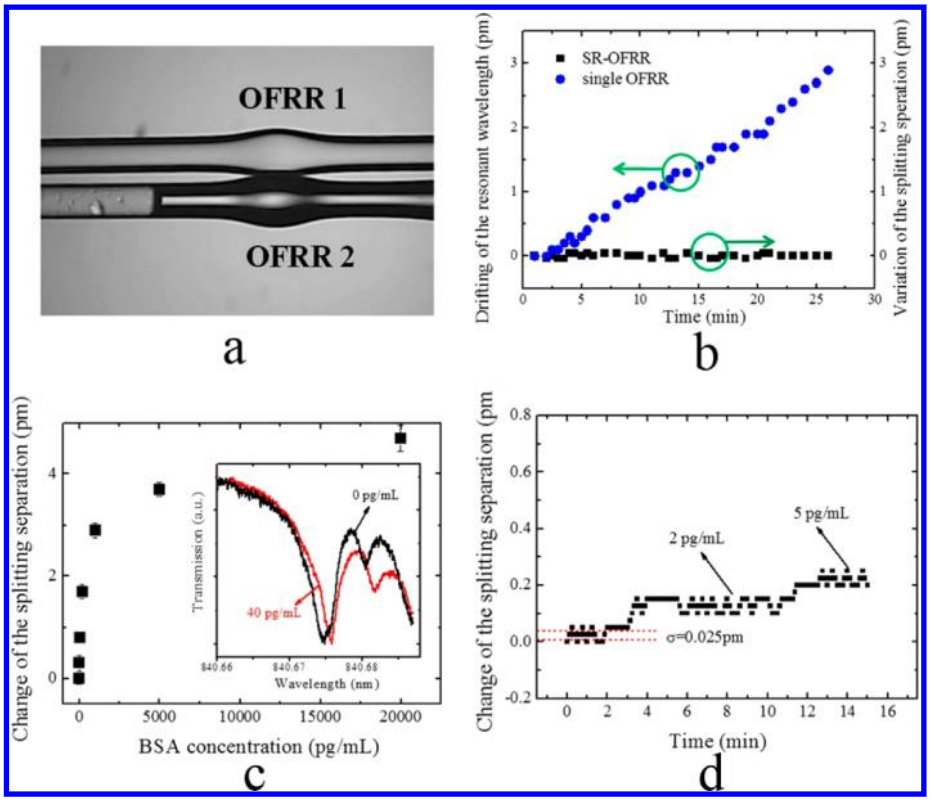

Figure 4. Thermal stability test: (a) picture of an SR-OFRR sensor, (b) stability test results of the SR-OFRR (black squares) and a single OFRR (blue circles). BSA detection results: (c) mode splitting as a function of the BSA concentration (the inset shows the splitting details with a BSA concentration of 0 pg/mL (black curve) and 40 pg/mL (red curve), respectively), (d) sensorgram for detection of BSA concentrations of 2 and 5 pg/mL, respectively. The resonance wavelength was near 840 nm.

OFRRs are identical, the noise caused by the environmental temperature fluctuation can be suppressed completely. With the increase in the diameter difference, the influence of temperature increases. Nevertheless, the maximal variation of the mode splitting separation is only 0.02 pm even when the diameter difference is 30 μm, which is well within the ring resonator fabrication capability. In contrast, the temperature change of 1 °C would cause a resonance wavelength drift as large as 11 pm for a single OFRR. In addition to temperature fluctuations, the laser frequency (or wavelength) jittering can cause the WGM spectral position to fluctuate. However, with the SR-OFRR the laser frequency jittering is completely canceled out regardless of the size difference between the two OFRRs and is therefore not reflected in the mode splitting measurement.

Thermal Stability Test. The fabrication and experimental setup for the SR-OFRR biosensor are described in detail in the Materials and Methods. A test for the noise-suppression capability of the SR-OFRR sensor was carried out at first. Figure 4a shows the picture of the SR-OFRR sensor. A single OFRR sensor was also used for comparison. The transmission spectra were monitored for 25 min for each sensor. As shown in Figure 4b, the resonance wavelength of the single OFRR drifted 3 pm as a result of the temperature and laser frequency fluctuations while the mode splitting of the SR-OFRR remained stable with a standard deviation of only 0.029 pm, 2 orders of magnitude lower than that of the single OFRR.

BSA Detection. Now we applied the SR-OFRR biosensor for analysis of actual attachment of protein molecules to the sensor surface, where BSA (molecular weight 66 400) was used as a model system. Note that there was no external noise-suppression technique employed in our measurement system during bimolecular detection.

Figure 4c shows the mode splitting with various BSA concentrations from 0 to 20 ng/mL. The inset shows the SR-OFRR spectra when the BSA concentration was 0 and 40 pg/mL, respectively. The difference between the two spectra is evident by the mode splitting. To further explore the detection limit, BSA solutions with concentrations of 2 pg/mL (~30 fM) and 5 pg/mL (~75 fM), which are much lower than that used in many other label-free optical biosensors, were gradually delivered through OFRR 2 for the detection. As shown in Figure 4d, a mode splitting of 0.1 pm can be clearly distinguished with 2 pg/mL BSA solution. Subsequent 5 pg/mL BSA solution resulted in an increase of 0.1 pm. The standard deviation, σ, was 0.025 pm, resulting in a noise equivalent detection limit (NEDL) of 0.5 pg/mL (~7.5 fM) for the BSA concentration. For an OFRR 2 with a radius of 140 μm, the effective sensor area of the inner surface was on the order of 10^3 μm^2. On the basis of our theoretical analysis discussed previously, as low as 10^3 BSA molecules are detectable.

Note that the standard deviation of 0.025 pm in the SR-OFRR obtained above arose mainly from the split mode line width and the residual common-mode noise. On the basis of the inset in Figure 4c, the Q-factor of the split mode in the SR-OFRR was approximately 3×10^5, which corresponded to a standard deviation of about 0.02 pm.[5] Therefore, the detection limit in our case is mainly determined by the spectral line width of the split mode. This is expected, as the common-mode noise has been significantly suppressed by the SR-OFRR. Con-

dx.doi.org/10.1021/ac402174x | Anal. Chem. 2013, 85, 9328−9332

sequently, by increasing the *Q*-factor of the split mode in the SR-OFRR, the detection limit can be further improved.

CONCLUSIONS

In summary, we have presented a detailed study of the SR-OFRR biosensor that has a high *Q*-factor and excellent immunity to the common-mode noises. Detection of binding of biomolecules as low as 2 pg/mL has been achieved with an NEDL of only 0.5 pg/mL. These results make the SR-OFRR-based label-free biosensor highly competitive, in comparison with the widely used ELISA (enzyme-linked immunosorbent assay)-based detection, whose detection limit is usually on the order of 1−10 pg/mL.

ASSOCIATED CONTENT

Supporting Information

Fabrication details, verification of the wall thickness, and complex transmission coefficient of SR-OFRR. This material is available free of charge via the Internet at http://pubs.acs.org.

AUTHOR INFORMATION

Corresponding Authors

*E-mail: xsfan@umich.edu.
*E-mail: lei_xu@fudan.edu.cn.

Author Contributions

[§]M.L. and X.W. contributed equally to this work.

Notes

The authors declare no competing financial interest.

ACKNOWLEDGMENTS

The work was supported by the National Natural Science Foundation of China (Grants 60977047, 60907011, 61078052, 61128011, and 11074051) and National Basic Research Program of China (973 Program) (Grant 2011CB921802).

REFERENCES

(1) Vollmer, F.; Arnold, S. *Nat. Methods* **2008**, *5*, 591−596.
(2) Fan, X. D.; White, I. M.; Shopova, S. I.; Zhu, H.; Suter, J. D.; Sun, Y. *Anal. Chim. Acta* **2008**, *620*, 8−26.
(3) Luchansky, M. S.; Bailey, R. C. *Anal. Chem.* **2012**, *84*, 793−821.
(4) Vollmer, F.; Yang, L. *Nanophotonics* **2012**, *1*, 267−291.
(5) Oates, T. C.; Burgess, L. W. *Anal. Chem.* **2012**, *84*, 7713−7720.
(6) Oates, T. C.; Burgess, L. W. *Appl. Spectrosc.* **2011**, *65*, 1187−1192.
(7) White, I. M.; Fan, X. D. *Opt. Express* **2008**, *16*, 1020−1028.
(8) Li, H.; Fan, X. D. *Appl. Phys. Lett.* **2010**, *97*, 011105.
(9) Lu, T.; Chen, T.; Herchak, S.; Kim, J.-H.; Fraser, S. E.; Flagan, R. C.; Vahala, K. *Proc. Natl. Acad. Sci. U.S.A.* **2011**, *108*, 5976−5979.
(10) Homola, J. *Chem. Rev.* **2008**, *108*, 462−493.
(11) Luff, B. J.; Wilkinson, J. S.; Piehler, J.; Hollenbach, U.; Ingenhoff, J.; Fabricius, N. *J. Lightwave Technol.* **1998**, *16*, 583−592.
(12) Prieto, F.; Sepúlveda, B.; Calle, A.; Llobera, A.; Domínguez, C.; Lechuga, L. M. *Sens. Actuators, B* **2003**, *92*, 151−158.
(13) Zhu, J. G.; Ozdemir, S. K.; Xiao, Y.-F.; Li, L.; He, L.; Chen, D.-R.; Yang, L. *Nat. Photonics* **2010**, *4*, 122−122.
(14) He, L. N.; Ozdemir, K.; Zhu, J. G.; Kim, W.; Yang, L. *Nat. Nanotechnol.* **2011**, *6*, 428−432.
(15) Arnold, S.; Dantham, V. R.; Barbre, C.; Garetz, B. A.; Fan, X. D. *Opt. Express* **2012**, *20*, 26147−26159.
(16) Grudinin, I. S.; Lee, H.; Painter, O.; Vahala, K. J. *Phys. Rev. Lett.* **2010**, *104*, 083901.
(17) Li, M.; Wu, X.; Liu, L.; Xu, L. *Opt. Express* **2013**, *21*, 16908−16913.
(18) Smith, D. D.; Chang, H. R.; Fuller, K. A. *J. Opt. Soc. Am. B* **2003**, *20*, 1967−1974.
(19) Shopova, S. I.; Sun, Y.; Rosenberger, A. T.; Fan, X. D. *Microfluid. Nanofluid.* **2009**, *6*, 425−429.